MgO Nanocrystals

DOI: 10.1002/anie.200902056

Size-Controlled Synthesis and Optical Properties of Monodisperse Colloidal Magnesium Oxide Nanocrystals**

*Hoi Ri Moon, Jeffrey J. Urban, and Delia J. Milliron**

Methods now exist to synthesize colloidal nanocrystals of a wide range of metals, chalcogenide and pnictide semiconductors, and some transition-metal oxides.[1] The resulting products exhibit a spectrum of size-dependent properties and are solvent dispersible for processing and integration. For example, uniform polymer–nanocrystal composites can be prepared by casting from a cosolution of the two components to achieve composite materials with high refractive index, bright luminescence, or nonlinear optical properties.[2] However, current solution-phase routes to alkaline earth metal oxide nanoparticles, such as MgO and CaO, initially yield the hydroxide precursors ($Mg(OH)_2$ and $Ca(OH)_2$) which must be calcined at high temperature to produce crystalline alkaline earth metal oxides.[3] Unfortunately, this process results in uncontrolled grain growth and sintering of the nanoparticles into partially fused, random nanocrystalline networks. Efforts to break apart the networked irregular powder and to disperse isolated nanocrystals using surfactants have resulted in aggregates 100 nm or larger with limited stability in dispersion.[4] Alternatively, vapor-phase methods such as chemical vapor deposition and combustion synthesis have been used to form MgO nanocrystals that are irrevocably bound to the substrate.[5] Here, we report the direct synthesis and optical characterization of colloidal magnesium oxide nanocrystals of narrow size distribution and diameters tunable from 2 to 8 nm. The impact of bound surfactants on the optical properties of the nanocrystals was investigated through chemical exchange of their surface ligands. The development of solvent-processible, size-tunable alkaline earth oxide nanocrystals opens up new opportunities in rational catalysis, gas separation, and nanooptics.

Solid films of alkaline earth oxides are commonly used in catalysis, either as a support for catalytically active metals such as Pt or Pd, or as an active catalytic surface.[3a,4,6] Colloidal nanocrystals circumvent the inevitable reduction in surface area that occurs during calcination and introduce the possibility of carrying out catalysis in stable dispersions.[7] Complementary to their established catalytic utility, alkaline earth oxide nanocrystals have potential optical applications. For example, MgO nanocrystals synthesized in the gas phase have been doped with calcium and transition-metal ions to yield either broad blue emission or spectrally narrow photoluminescence, respectively.[5] The bright blue emission we now report for colloidal MgO nanocrystals, not observed in bulk MgO crystals, offers an inexpensive, attractive alternative for optical applications.

MgO nanocrystals were synthesized from an organometallic precursor, bis(cyclopentadienyl)magnesium [Cp_2Mg], and trioctylphosphine oxide (TOPO) in distilled benzyl ether. Briefly, a solution containing [Cp_2Mg] (308 mg, 2 mmol) and TOPO (80 mg, 0.2 mmol) in benzyl ether (4 mL) was vigorously stirred and heated to 285 °C for 2 hours under N_2 then immediately cooled to room temperature. Methanol was added to flocculate the nanocrystals, which were subsequently separated by centrifugation. The MgO nanocrystals could then be redispersed in a broad range of organic solvents, such as toluene and chloroform.

X-ray diffraction of the nanocrystals (Figure 1 a) indicates that the product is single-phase cubic MgO of the $Fm\bar{3}m$ space group (JCPDS 89-7746). Remarkably, none of the common synthetic side products such as $Mg(OH)_2$ or $MgCO_3$ are observed. The positions of the (200) and (220) reflections are

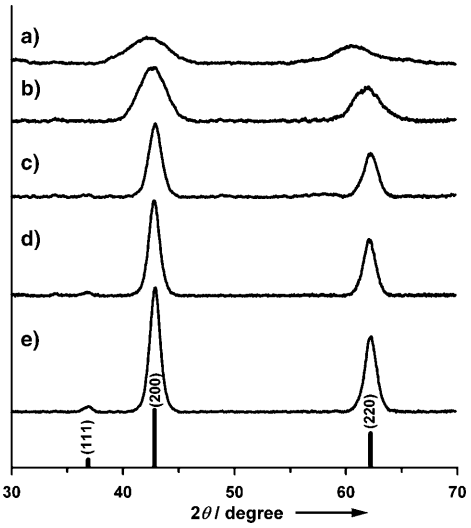

Figure 1. X-ray diffraction patterns of MgO nanocrystals synthesized with a) no added water, or b) 5 μL, c) 10 μL, d) 20 μL, and e) 40 μL of added water to standard reaction conditions described in the text. Patterns are indexed according to cubic MgO (JCPDS 89-7746).

[*] Dr. H. R. Moon, Dr. J. J. Urban, Dr. D. J. Milliron
The Molecular Foundry, Lawrence Berkeley National Laboratory
1 Cyclotron Road, MS 67R4110, Berkeley, CA 94720 (USA)
Fax: (+1) 510-486-6166
http://foundry.lbl.gov
E-mail: dmilliron@lbl.gov

[**] We thank S. Swanson and Dr. T. Topuria of the IBM Almaden Research Center, as well as R. Zhang, for research contributions during the initial phases of this work. Work at the Molecular Foundry was supported by the Office of Science, Office of Basic Energy Sciences, of the U.S. Department of Energy under Contract No. DE-AC02-05CH11231. H.R.M. is supported under B&R code KC0202020, Hydrogen Storage program.

Supporting information for this article is available on the WWW under http://dx.doi.org/10.1002/anie.200902056.

shifted to lower angle than bulk MgO and are noticeably broadened, clearly indicating the formation of MgO nanocrystals of very small size and expanded lattice. The size of the nanocrystals is estimated by applying the Debye–Scherrer equation to the (200) reflection, correcting for instrumental broadening. The derived crystallite diameter is 2.1 nm, somewhat smaller than that estimated by transmission electron microscopy (TEM).

The shape, size, and crystal structure of the MgO nanocrystals were confirmed by both low- and high-resolution TEM (Figures 2 and 3, respectively). We note that the low electron density of MgO (low atomic number) combined with the small size of these nanocrystals severely limits the contrast in low-resolution imaging. Figure 2a shows a representative TEM image of the approximately spherical nanocrystals. Their diameter cannot be quantitatively ascertained unambiguously because of the low contrast but it is estimated to be (4.5 ± 0.3) nm (a histogram of particle diameters is presented in Figure S1 in the Supporting Information). The nanocrystals lie in random orientations on the carbon support film, resulting in particle-to-particle variation diffractive contrast variation in low-resolution TEM images and in the observation of different zone axes in high-resolution TEM images. Projections of the rock-salt lattice along the [100] and [$\bar{1}$10] directions are clearly observed (Figure 3), and each particle is a single crystal, with no amorphous surface layer.

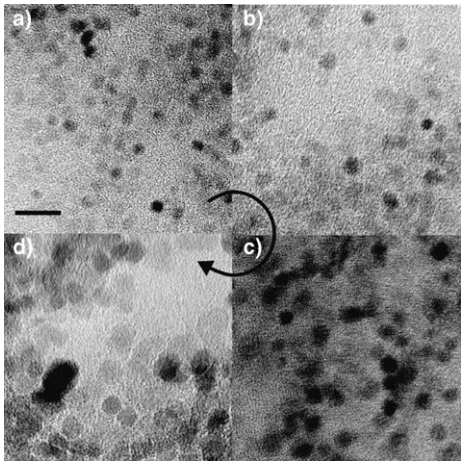

Figure 2. Low-resolution TEM images of MgO nanocrystals synthesized with a) no added water, or with b) 5 μL, c) 10 μL, and d) 20 μL of added water. The bar in (a) indicates 20 nm. Nanocrystal diameter increases systematically with added water, as evident from following the curved arrow.

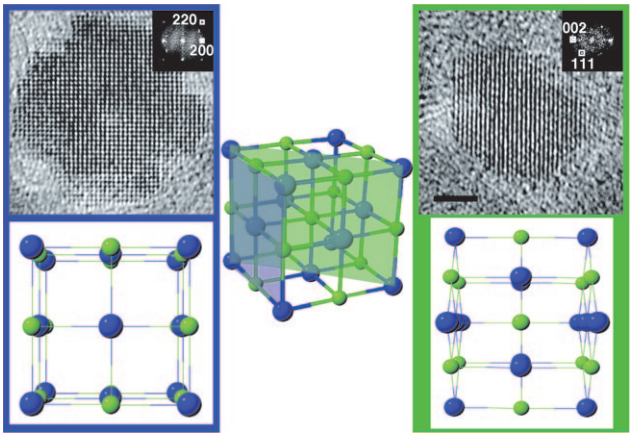

Figure 3. High-resolution TEM images of MgO nanocrystals oriented along the [100] (left) and [$\bar{1}$10] (right) zone axes, and the corresponding Fourier transforms. The bar indicates 2 nm and, in the Fourier transforms, one spot of each symmetry-related group is indexed according to the rock-salt structure.

The size of the MgO nanocrystals was controlled by systematically varying the reaction conditions. Addition of increasing, yet substoichiometric, amounts of H_2O to the reaction solution prior to heating yielded nanocrystals with increasingly larger diameters. The size derived from XRD peak broadening increased with the amount of H_2O added: 2.1 nm (0 μL), 3.0 nm (5 μL), 6.4 nm (10 μL), and 7.6 nm (20 μL) (Figure 1a–d and Table S1 in the Supporting Information). TEM results (Figure 2 and Figure S1 in the Supporting Information) are consistent with this trend and show that the spherical shape and narrow size distribution is maintained. The rounded shape of these nanocrystals differs from the highly faceted cubes formed by CVD.[5] This difference, potentially significant for catalytic and optical properties, can be ascribed to the smaller size of the colloidal particles and their termination with organic ligands. For example, PbTe shares the rock-salt crystal structure of MgO, and colloidal PbTe is nominally spherical below approximately 10 nm in diameter, forming faceted cubes at larger sizes.[8] The size does not increase significantly further when more H_2O (40 μL) is added (Figure 1e, deduced crystallite size 8.0 nm), and the shape and size become less regular (Figure S2 in the Supporting Information).

Although bulk, single-crystalline MgO is a wide-band-gap insulator ($E_g > 7$ eV), optical transitions in the visible range have been observed in CVD-synthesized MgO nanocrystals and assigned to surface states.[5] These colloidal MgO nanocrystals exhibit a broad absorption band, which is centered around 325 nm and extends well into the visible range (Figure 4a). The absorption peak is slightly red-shifted at larger sizes, likely because of changing contributions from surface states associated with surface F-centers or with low-coordinate oxygen anions, whose energies cover a broad, sub-band gap range.[5,9] The nanocrystals' photoluminescence (PL) is centered around 440 nm, again shifting slightly with size (Figure 4b). Unlike CVD-grown MgO nanocrystals, which surface doping with Ca^{2+} ions to luminesce brightly, these colloidal nanocrystals have a quantum yield of 15–19%, falling off slightly at larger sizes (for details see Table S2 in the Supporting Information). Neither the absorption nor photoluminescence are consistent with any of reagents employed in the synthesis of the nanocrystals (Figure S3 in the Supporting Information). We suggest that the large population of surface states on these small nanocrystals is responsible for the efficient blue emission, which is obvious to the naked eye.

Because surface states are thought to dominate the optical properties, FTIR spectroscopy was used to discern the nature of the surface-coordinating organic capping groups that facilitate dispersion of the nanocrystals in organic solvents.

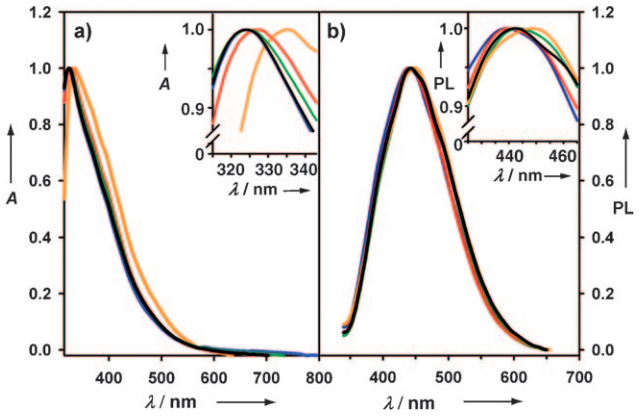

Figure 4. a) Optical absorption and b) photoluminescence (PL) spectra of MgO nanocrystals obtained by varying the amount of water in the reaction, recorded in toluene dispersion. Water amount: 0 μL (black), 5 μL (blue), 10 μL (green), 20 μL (red), and 40 μL (orange). PL spectra were collected under excitation at 335 nm.

Based on the reagents included in the reaction solution, we consider three likely candidates: benzyl ether, TOPO, and tri(*n*-octyl)phosphine (TOP), produced as a side product. Benzyl ether is easily distinguished from TOPO or TOP by examining the C–H stretch region of the FTIR spectra (Figure 5). The former is dominated by aromatic C–H bonds at high stretching frequency, with a small contribution from methylene C–H bonds at lower frequency (Figure 5c). In contrast, TOP and TOPO are characterized by methylene C–H stretching bands, with a smaller peaks arising from methyl C–H stretches (Figure 5d). FTIR spectra for TOP and TOPO differ most notably in the strong P=O stretching peak, appearing at 1144 cm^{-1} for neat TOPO (Figure 5d). This peak is, however, known to shift when TOPO binds to nanocrystal surfaces,[8] and a similar peak might be anticipated for TOP bound to surface oxygen atoms.

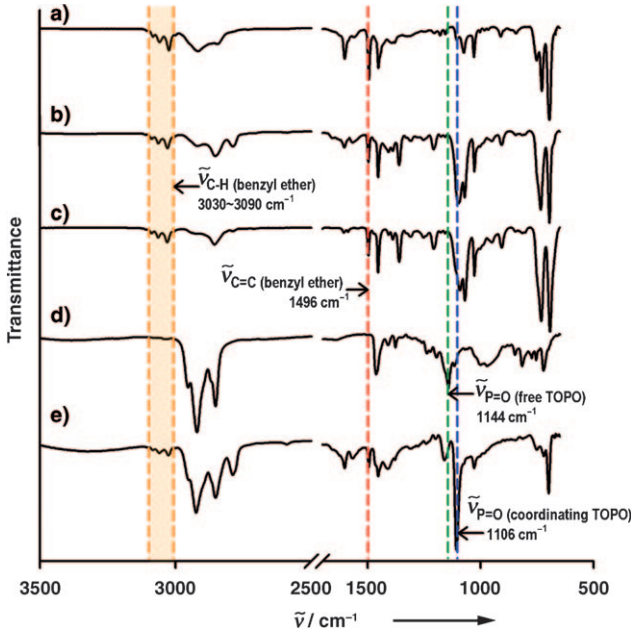

Figure 5. FTIR spectra of a) MgO nanocrystals as-synthesized, and following ligand exchange with b) benzyl ether and with e) TOPO. For comparison, spectra of neat c) benzyl ether and d) TOPO are included.

The FTIR spectrum of the as-synthesized MgO nanocrystals exhibit clear evidence of benzyl ether coordination. The C–H stretch region is dominated by aromatic bands, no P=O stretching band is apparent, and the C=C stretch at 1496 cm^{-1} is clearly visible (Figure 5a). To confirm this assignment, ligand exchange was carried out to displace the original surface ligands and to coat the surface specifically with either TOPO or benzyl ether. While the spectrum is effectively unchanged following ligand exchange with benzyl ether (Figure 5b), new peaks dominate the spectrum after TOPO exchange (Figure 5e). Methylene bands now dominate the C–H stretch region and a peak at 1106 cm^{-1}, assigned to surface coordinated P=O,[10] appears. Weak aryl C–H and C=C stretching bands are evidence of residual benzyl ether. Thus, the as-synthesized MgO nanocrystals are coated with benzyl ether, and ligand exchange can be carried out to partially displace these ligands with TOPO. Furthermore, the photoluminescence quantum yield of the TOPO-exchanged nanocrystals was 50% less than that of the original nanocrystals while benzyl ether exchange had a negligible effect on the photoluminescence. The efficient photoluminescence therefore depends not only on the population of surface states, but also on their interaction with the coordinated ligands. However, on the basis of these initial observations, we cannot discern the specific role that ligands play in the observed luminescence.

We have successfully synthesized monodisperse colloidal nanocrystals of the alkaline earth metal oxide MgO, using added H_2O to control the diameter in the 2–8 nm range. Very small MgO nanocrystals could be synthesized from the reaction of [Cp_2Mg] with benzyl ether alone (Figure S4 in the Suporting Information), but TOPO and H_2O facilitate the production of nanocrystals with larger diameters. The resulting nanocrystals are single crystalline, and they exhibit size-dependent and efficient blue luminescence. Their benzyl ether capping ligands facilitate dispersion in organic solvents and can be easily exchanged to tune surface chemistry and optical properties. These nanocrystals also create new opportunities for rationally investigating and carrying out catalysis in colloidal dispersions.

Experimental Section

Preparation of MgO nanocrystals: Tri(*n*-octyl)phosphine oxide (TOPO) was dried at 130°C for 3 h under vacuum, and benzyl ether was distilled over CaH_2, then both were stored in a nitrogen glove box maintained at <1 ppm O_2 and H_2O. [Cp_2Mg] (308 mg, 1.99 mmol), TOPO (80 mg, 0.21 mmol), and benzyl ether (4 mL) were mixed and stirred magnetically at room temperature for 2 h under inert atmosphere. The reaction mixture was heated to 285°C and subsequently maintained at that temperature for 2 h. The color of the solution changed from orange to dark brown. After the reaction mixture had cooled to room temperature, methanol (30 mL) was added to yield a brown flocculate, which was separated from the solution by centrifugation (9000 rpm, 20 min). The resultant brown product was redissolved in toluene (4 mL) and again flocculated with

methanol (20 mL), and a powder comprising MgO nanocrystals was finally obtained by centrifugation (9000 rpm, 20 min). The recovered nanocrystals could be redispersed in toluene.

Effect of H_2O on the formation of MgO nanocrystals: A mixture of $[Cp_2Mg]$ (308 mg, 2.0 mmol), TOPO (76 mg, 0.20 mmol), and benzyl ether (4 mL) was stirred magnetically at room temperature for 2 h under inert atmosphere, as described above. To the solution was added 5 (0.28 mmol), 10 (0.56 mmol), 20 (1.11 mmol), or 40 μL (2.22 mmol) of H_2O, respectively, followed by heating to 285 °C. The isolation and recovery of nanocrystals proceeded as described above.

Ligand exchange with benzyl ether: As-prepared MgO nanocrystals dispersed in toluene (1 mL, ≈40 wt %) were added to benzyl ether (4 mL), and the solution was stirred and heated at 80 °C for 18 h under nitrogen. After the reaction mixture had cooled to room temperature, an excess of methanol (20 mL) was added to induce flocculation of the nanocrystals, which were separated from the solution by centrifugation (9000 rpm, 30 min). The resultant brown product could be redispersed in toluene.

Ligand exchange with TOPO: As-prepared MgO nanocrystals dispersed in toluene (1 mL, ≈40 wt %) were mixed with TOPO (140 mg, 0.35 mmol). After stirring for 18 h at 80 °C under nitrogen, the solution was cooled to room temperature. The ligand-exchanged nanocrystals were flocculated by the addition of methanol (10 mL) and separated from the solution by centrifugation (9000 rpm, 30 min). The brown product could be redispersed in toluene.

Nanocrystal characterization: The size and morphology of MgO nanocrystals were probed by high-resolution transmission electron microscopy (HRTEM) using a JEOL 2100F instrument operating at 200 kV. Samples for TEM analysis were prepared by drying a drop of toluene solution containing the nanocrystals on the surface of a carbon-coated copper grid. XRD patterns were obtained using a Bruker D8 Discover X-ray diffractometer with a general area detector diffraction system (GADDS) using $Cu_{K\alpha}$ radiation ($\lambda =$ 0.154 nm) from samples prepared by depositing precipitated powders on a quartz plate. An alumina plate (SRM 1976-National Institute of Standard Technology) powder standard pattern was obtained to determine the instrumental broadening, and peaks were fit to a Gaussian function. Infrared spectra were recorded on a Perkin-Elmer FTIR Spectrum One spectrophotometer. Absorption spectra were obtained with a Shimadzu UV-3600 UV/VIS/NIR Spectrophotometer. Photoluminescence spectra were recorded on a Jobin Yvon Horiba Fluorolog 3, and an integrating sphere employed to measure absolute quantum yields.

Received: April 17, 2009
Revised: May 23, 2009
Published online: July 20, 2009

Keywords: colloids · luminescence · metal oxides · nanocrystals · synthesis design

[1] a) J. Park, J. Joo, S. G. Kwon, Y. Jang, T. Hyeon, *Angew. Chem.* **2007**, *119*, 4714 – 4745; *Angew. Chem. Int. Ed.* **2007**, *46*, 4630 – 4660; b) S. G. Kwon, T. Hyeon, *Acc. Chem. Res.* **2008**, *41*, 1696 – 1709; c) Y. Yin, A. P. Alivisatos, *Nature* **2005**, *437*, 664 – 670; d) M. Niederberger, G. Garnweitner, *Chem. Eur. J.* **2006**, *12*, 7282 – 7302.

[2] a) L. Bakueva, S. Musikhin, M. A. Hines, T.-W. F. Chang, M. Tzolov, G. D. Scholes, E. H. Sargent, *Appl. Phys. Lett.* **2003**, *82*, 2895 – 2897; b) D. E. Fogg, L. H. Radzilowski, B. O. Dabbousi, R. R. Schrock, E. L. Thomas, M. G. Bawendi, *Macromolecules* **1997**, *30*, 8433 – 8439; c) P. P. Pompa, L. Matiradonna, A. Della Torre, L. Carbone, L. L. del Mercato, L. Manna, M. De Vittorio, F. Calabi, R. Cingolani, R. Rinaldi, *Sens. Actuators B* **2007**, *126*, 187 – 192; d) P. K. Sudeep, T. Emrick, *Polym. Rev.* **2007**, *47*, 155 – 163.

[3] a) K. Zhu, J. Hu, C. Kübel, R. Richards, *Angew. Chem.* **2006**, *118*, 7435 – 7439; *Angew. Chem. Int. Ed.* **2006**, *45*, 7277 – 7281; b) O. B. Koper, I. Lagadic, A. Volodin, K. J. Klabunde, *Chem. Mater.* **1997**, *9*, 2468 – 2480; c) P. P. Fedorov, E. Tkachenko, S. V. Kuznetsov, V. V. Voronov, S. V. Lavrishchev, *Inorg. Mater.* **2007**, *43*, 502 – 504; d) W. Wang, X. Qiao, J. Chen, H. Li, *Mater. Lett.* **2007**, *61*, 3218 – 3220; e) C. Yan, D. Xue, *J. Phys. Chem. B* **2005**, *109*, 12358 – 12361.

[4] P. Jeevanandam, K. J. Klabunde, *Langmuir* **2003**, *19*, 5491 – 5495.

[5] a) S. Stankic, M. Sterrer, P. Hofmann, J. Bernardi, O. Diwald, E. Knozinger, *Nano Lett.* **2005**, *5*, 1889 – 1893; b) I. S. Altman, P. V. Pikhitsa, M. Choi, J. I. Jeong, H.-J. Song, I. E. Agranovski, T. E. Bostrom, *Appl. Phys. Lett.* **2003**, *83*, 3689 – 3691; c) I. S. Altman, P. V. Pikhitsa, M. Choi, H.-J. Song, A. G. Nasibulin, E. I. Kauppinen, *Phys. Rev. B* **2003**, *68*, 125324.

[6] a) G. W. Wagner, P. W. Bartram, O. Koper, K. J. Klabunde, *J. Phys. Chem. B* **1999**, *103*, 3225 – 3228; b) P. K. Stoimenov, V. Zaikovski, K. J. Klabunde, *J. Am. Chem. Soc.* **2003**, *125*, 12907 – 12913; c) J. Hu, K. Zhu, L. Chen, C. Kübel, R. Richards, *J. Phys. Chem. C* **2007**, *111*, 12038 – 12044.

[7] R. Narayanan, M. A. El-Sayed, *Nano Lett.* **2004**, *4*, 1343 – 1348.

[8] J. E. Murphy, M. C. Beard, A. G. Norman, S. P. Ahrenkiel, J. C. Johnson, P. Yu, O. I. Mićić, R. J. Ellingson, A. J. Nozik, *J. Am. Chem. Soc.* **2006**, *128*, 3241 – 3247.

[9] a) A. L. Shluger, P. V. Sushko, L. N. Kantorovich, *Phys. Rev. B* **1999**, *59*, 2417 – 2430; b) V. I. Avdeev, G. M. Zhidomirov, *J. Struct. Chem.* **2003**, *44*, 918 – 926.

[10] a) J. E. B. Katari, V. L. Colvin, A. P. Alivisatos, *J. Phys. Chem.* **1994**, *98*, 4109 – 4117; b) A. G. Young, N. Al-Salim, D. P. Green, A. J. McQuillan, *Langmuir* **2008**, *24*, 3841 – 3849.

